ELSEVIER

15 December 1998

Optics Communications 158 (1998) 313–321

OPTICS COMMUNICATIONS

Full length article

Spatio-temporal dynamics in vertical cavity surface emitting lasers excited by fast electrical pulses

M. Giudici [a,1], J.R. Tredicce [a], G. Vaschenko [b], J.J. Rocca [b], C.S. Menoni [b]

[a] *Institut Non Lineaire de Nice, Université de Nice-Sophia-Antipolis, CNRS UMR, 06560 Valbonne, France*

[b] *Center for Optoelectronic Computing Systems and Department of Electrical Engineering, Colorado State University, Fort Collins, CO 80523, USA*

Received 25 February 1998; revised 10 June 1998; accepted 11 June 1998

Abstract

We have measured the time average spatial intensity distribution and the spatio-temporal evolution of the spectrally resolved radiation emitted from broad-area vertical cavity surface emitting lasers (VCSEL) when pumped by a fast current pulse. We show that an intrinsic symmetry break exists due to geometrical asymmetry of the device structure and that the frequency separation between different modes allows the evaluation of the asymmetry factor. The space–time behavior shows the appearance of higher-order modes coexisting or alternating in time. The dynamical behavior shows a chirping in frequency.

1. Introduction

Space–time dynamics of lasers has been the subject of increased interest in the last several years. Spontaneous breaking of the spatio-temporal symmetry leading to complexity has been investigated both theoretically and experimentally [1–3]. Theoretical works predict the existence of topological defects [4]. Topological defects may give rise to defect-mediated turbulence as observed in photorefractive materials [5]. However, to date, there is no experimental evidence of their existence in lasers [6,7]. It was conjectured that the interaction of longitudinal and transverse modes of the cavity in large Fresnel number lasers might be responsible for the disagreement among theoretical and experimental results. All theoretical models take into consideration transverse modes of a single longitudinal mode. However, the gain bandwidth in most lasers experimentally studied is large enough for both longitudinal and transverse modes to interact when the Fresnel number is high enough to observe spatial complexity. In that sense, vertical surface emitting lasers (VCSEL) represent a good test bench to study space–time complexity in lasers. Their short cavity length does not allow for multi-longitudinal mode operation and therefore they fulfil, in principle, the assumptions of the theory. Preliminary results obtained on 25×25 μm VCSELs showed the existence of very complex spatial intensity distributions [8–10]. However, a detailed analysis is not yet available. On the other hand, transient build-up of low-order transverse modes and their interaction was recently studied experimentally in Refs. [11,12]. It was shown there that, close to the laser threshold, the appearance or non-appearance of a transverse mode depends, among other factors, on the initial conditions. From a theoretical point of view, cw operation of low-order modes is well described in Ref. [13]. In this paper we report the experimental analysis of the time-averaged and time-resolved intensity spatial distribution in VCSELs with different values of Fresnel number under pulsed pumping. We also studied the influence of the initial conditions on the spatio-temporal dynamics.

[1] Corresponding author. E-mail: giudici@inln.cnrs.fr

0030-4018/98/$ - see front matter
PII: S0030-4018(98)00326-5

2. Experimental set-up

We studied the dynamics of GaAs/AlGaAs multiple quantum well VCSELs having distributed Bragg reflectors (DBR) of AlAs/AlGaAs step graded layers composed of 19 and 29 periods for the p-doped top and n-doped bottom mirrors, respectively. The emission wavelength peaked at 840 nm. Active region diameter devices of 15, 18, 22 and 24 μm with top contact window diameter of 12, 15, 18 and 20 μm, respectively, were tested in the experiment. Gain guiding was achieved through ion implantation in the top DBR region. The VCSELs were DC biased through a bias tee and were electrically pulsed by a fast pulse generator that produced square pulses with a duration of 0.3–1 ns at a rate of 80 MHz with a risetime of 100–200 ps and variable amplitude.

The spatio-temporal dynamics of the VCSELs was obtained using the experimental set-up schematically illustrated in Fig. 1. Good spatial resolution was reached by expanding and collimating the output of the lasers using a 20× microscope objective. Spectral resolution was obtained sending the expanded laser beam through a half-meter focal length monochromator (Jarell Ash 82-020). With the dispersion introduced by the monochromator it was possible to detect the dynamical evolution of each single transverse mode, avoiding their overlap in the detector. In order to detect the spatio-temporal distribution of the VCSEL output with high temporal resolution, a synchroscan streak-camera was used. The streak tube generated frames ('streak images') in which the horizontal axis represents the spatial coordinate along a slit placed in front of the photocathode, and the vertical axis represents time. Therefore, the intensity distribution in the streak image represents the space–time distribution of the laser light intensity along of a horizontal slice of the laser beam. The streak tube had an S-20 photocathode and a P-20 phosphorous screen. A fiber-optics-coupled image intensifier was used to intensify the output of the streak tube. The intensified image was detected with a two-dimensional cooled CCD array, and was displayed with a graphics software that generates a two-dimensional picture in which a grey-level scale represents the intensity distribution. The streak-camera scans and the pulse generator were synchronized by an 80 MHz signal from an RF synthesizer. The resolution of the streak-camera is better than 10 ps for streaks having a span of 1.3 ns. The entire two-dimensional space distribution of the laser intensity in each mode was also observed by directing part of beam to a second CCD detector array by means of a beam splitter placed in front of the streak camera.

3. Results and discussion

In Fig. 2 we show the time-averaged spatial distribution of the laser intensity at different wavelengths. The mea-

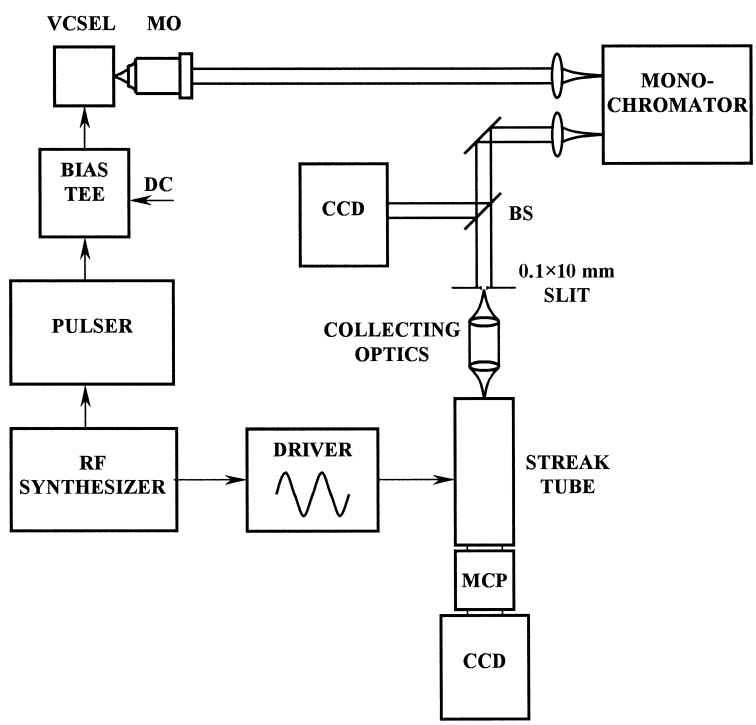

Fig. 1. Experimental set-up: MO collimator, BS 50/50 beam splitter, MCP multi-channel plate, CCD ccd detector.

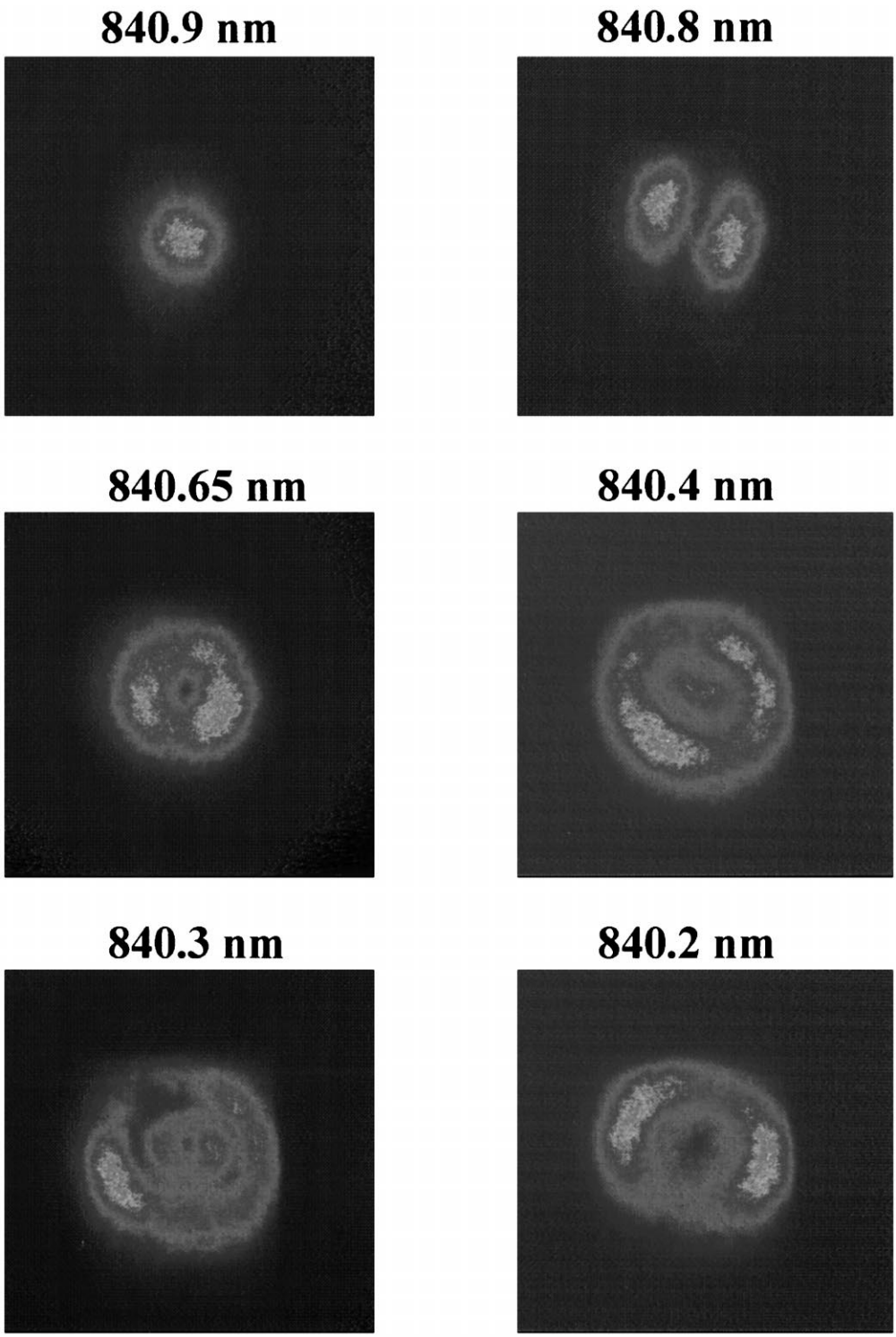

Fig. 2. Time-averaged spatial distribution of the laser intensity at different wavelengths. The VCSEL active region is 18 μm in diameter, it is DC biased at 80% of threshold current (I_{th}) and it is excited above threshold by a pulse of 400 ps width and 14 times I_{th} amplitude. The intensity is represented on a grey scale. The maximum level is different for each picture in order to enhance the contrast. Black corresponds to zero intensity level (background), while white corresponds to the following intensity levels (arbitrary units): 2000 for 840.9 nm, 2000 for 840.8 nm, 4500 for 840.65 nm, 500 for 840.4 nm, 2500 for 840.3 nm, 200 for 840.2 nm.

surements were performed on lasers with circular apertures varying from 15 to 24 μm. Qualitatively the results were not dependent on the laser aperture diameter in the available range. A radially symmetric, and almost Gaussian distribution is observed at 840.9 nm. There is no laser emission at higher wavelengths. Instead at lower wavelengths we observed the appearance of the first-order transverse mode (Fig. 2, 840.8 nm) with a non-radially symmetric intensity distribution. In principle such distribution can be associated with a linear combination of the TEM_{0+1}^{+1} and TEM_{0+1}^{-1} modes of a Gauss–Laguerre basis. The field can be written in the form [3]:

$$E(r,\theta,t) = f(r)(e^{i\theta} + e^{-i\theta})\, e^{-i\omega_1 t} = E_1(r,\theta,t) + E_2(r,\theta,t), \quad (1)$$

where (r,θ) are the polar coordinates in the plane transverse to the direction of propagation of the electromagnetic field and ω_1 is the operating frequency for the modes defined by $f(r)$. This experimental result is somehow surprising if we take into consideration the usual laser theory. In fact, using the well-known Maxwell equations, and reducing them to a normal form, we can write equations for each mode E_1 and E_2. We get [14]:

$$\partial_t E_1 = \mu E_1 - A E_1\left(|E_1|^2 + \alpha |E_2|^2\right),$$
$$\partial_t E_2 = \mu E_2 - A E_2\left(|E_2|^2 + \alpha |E_1|^2\right), \quad (2)$$

where μ and A are complex and depend on laser parameters like gain and loss rates. The coupling constant α can be exactly calculated for homogeneously broadened lasers and it is equal to 2. For inhomogeneously broadened lasers, α is smaller than 2 but always greater than 1 [15].

For α larger than 1, the solution $|E_1| = |E_2| \neq 0$ is unstable and therefore it should not appear if usual laser theory applies. Instead this solution has been experimentally observed at 840.8 nm (Fig. 2). The disagreement may have two origins: the normal form taken into consideration does not apply to VCSELs or the circular symmetry is substantially broken by geometrical factors or inhomogeneities. However, to our knowledge, the normal form applies well to all models previously used for VCSELs [16]. It is then generally accepted that unavoidable manufacturing imperfections break the intrinsic O_2 symmetry of the system. In such a case Eqs. (2) can be written as [17]:

$$\partial_t E_1 = \mu E_1 - A\left(E_1\left(|E_1|^2 + \alpha |E_2|^2\right) - \varepsilon E_2\right),$$
$$\partial_t E_2 = \mu E_2 - A\left(E_2\left(|E_2|^2 + \alpha |E_1|^2\right) - \varepsilon E_1\right), \quad (3)$$

where ε is the asymmetry parameter. If $\varepsilon = 0$ we recover the O_2 symmetry, while $\varepsilon = 1$ means maximum symmetry breaking. In this case, the only possible solution of Eqs. (3) is the standing wave. An equivalent way to understand the physical implications and to evaluate the parameter ε is to consider the Hermite–Gauss basis. In this case (Fig. 2, 840.8 nm) can be interpreted as the mode TEM_{10} which has the form

$$E_{10}(r,\theta,t) = f(r)\sin(\theta)\, e^{(i\omega_1 t)}. \quad (4)$$

For $\varepsilon = 0$ this mode is degenerate in frequency with the TEM_{01} mode

$$E_{01}(r,\theta,t) = f(r)\sin(\theta)\, e^{(i\omega_1 t + \pi/2)}. \quad (5)$$

A radially symmetric intensity distribution is the result of having $|E_{10}| = |E_{01}|$. The fact that only one of them appears at 840.8 nm can be interpreted as due to the breaking of the degeneracy of the two modes that have different operating wavelengths. If $\varepsilon = 1$ we have the maximum separation in frequency among the two Hermite–Gauss modes and it corresponds to $1/2$ of the free spectral range of the cavity. In fact, at shorter wavelength (840.65 nm, Fig. 2) the intensity distribution becomes a ring evidencing the excitation of the TEM_{01} mode. Thus ε can be estimated to be of the order of 0.15 nm/840 nm $\approx 10^{-4}$. The wavelength corresponding to the TEM_{01} mode allows us to evaluate the frequency difference with respect to the fundamental mode which is ≈ 100 GHz. In the usual theory of Fabry–Perot cavities such separation in frequency between transverse modes corresponds to radius of curvature of the mirrors of 0.04 m. It is worthwhile to notice that the passage from the pure TEM_{01} mode to a mixed state with a TEM_{10} mode is a Hopf bifurcation which gives rise to oscillations at the frequency difference (≈ 60 GHz). At shorter wavelength we show some spatial intensity distributions which can be associated to higher-order transverse modes, like the TEM_{10} mode (840.4 nm, Fig. 2), the TEM_{02} mode (840.2 nm, Fig. 2) in the Gauss–Laguerre basis. In principle these results are not surprising, except for two observations:

1. At wavelength of 840.3 nm, thus between the TEM_{10} and TEM_{02} modes, a spatial distribution similar to the TEM_{11} appears. Other spatial distributions characterized by a single 'ring' and a large central area with vanishing intensity are observed around the minimum operating wavelengths (less than 840.2 nm up to 839.2 nm). These anomalous spatial intensity distributions, not shown in Fig. 2, could be associated to spatial inhomogeneous pumping or to the presence of gain even for a non-resonant frequency of the cavity, and therefore strong non-linear effects inside the medium.
2. The frequency spacing among consecutive transverse modes is not constant. This phenomena could be associated to different mode-pulling for each mode. In usual high Fresnel number lasers the effect is very small for low-order modes and increases with the mode order because of the higher losses. However, the separation in frequency must, in theory, decrease while in our VCSELs it increases. Another possible interpretation is a frequency shift taking place as the laser pulse develops.

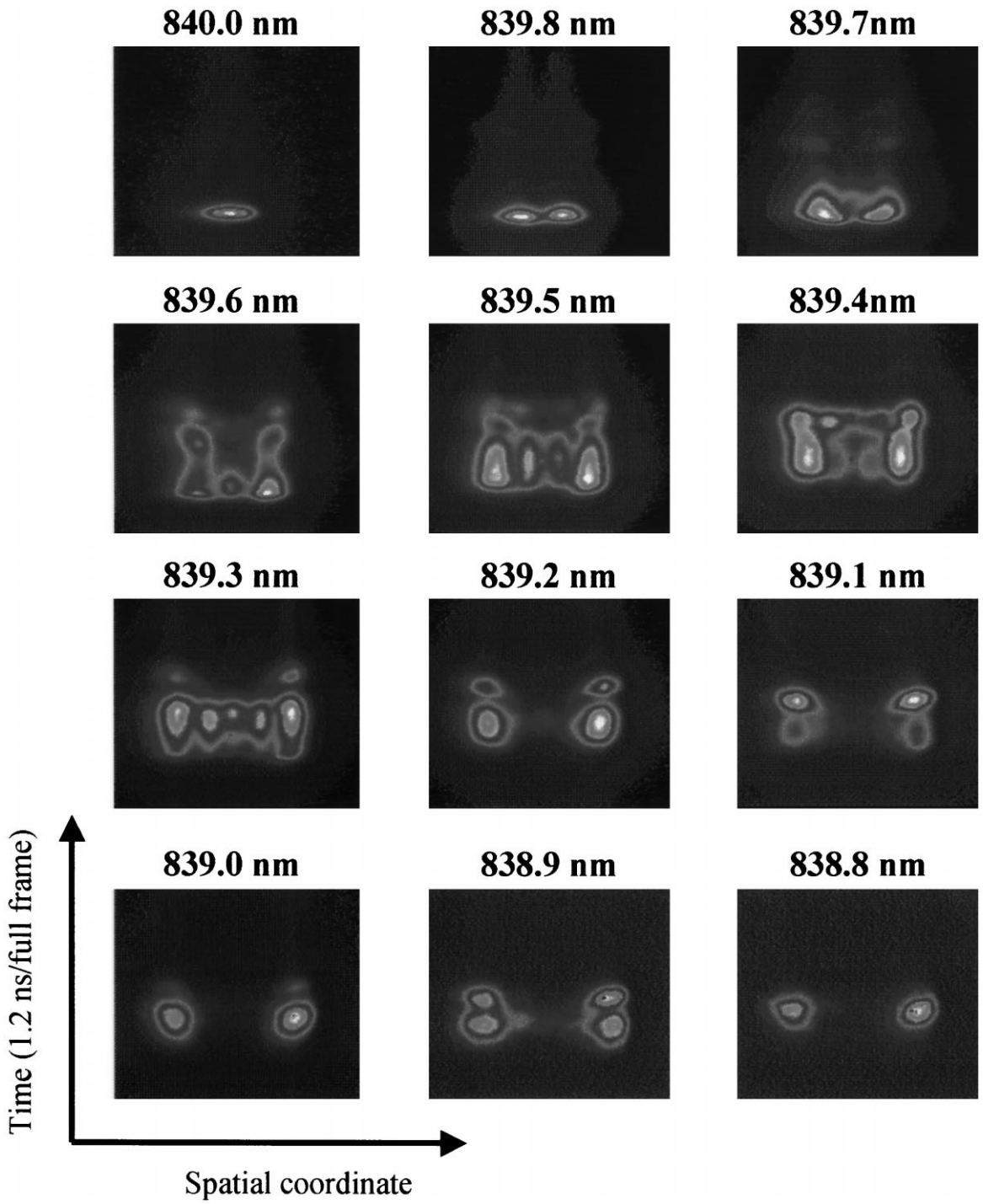

Fig. 3. Time-resolved horizontal cross-sections of the laser beam at different wavelengths. The VCSEL active region is 22 μm in diameter, it is DC biased at 10% of I_{th} and excited by a pulse of 400 ps width and $14 \times I_{th}$ amplitude. The time span is 1.235 ns. The intensity is represented on a grey scale. The maximum level is different for each picture in order to enhance the contrast. Black corresponds to zero intensity level (background), while white corresponds to the following intensity levels (arbitrary units): 2000 for 840.0 nm, 5500 for 839.8 nm, 4000 for 839.7 nm, 2500 for 839.6 nm, 3500 for 839.5 nm, 2500 for 839.4 nm, 3000 for 839.3 nm, 2000 for 839.2 nm, 1000 for 839.1 nm, 1000 for 839.0 nm, 250 for 838.9 nm, 250 for 838.8 nm.

Summarizing, the measurement of the time averaged spatial distribution resolved in wavelength indicates that relatively large area VCSEL tends to create spatial structures that could be interpreted as linear combination of usual cavity modes. Thus, there are not 'turbulent' structures with the presence of topological defects, even in the fast pulsing regime. Further information can be obtained by measuring the time-resolved intensity at different wavelengths.

We performed a series of measurements for different initial conditions and different excitation pulse durations and amplitudes for each available VCSEL. In general the qualitative dynamical behavior is independent of the excitation pulse amplitude and the laser diameter. However, the results can be divided in two groups depending on the initial conditions: laser below or above threshold before the excitation pulse. In Fig. 3 we show the time-resolved intensity patterns appearing at different wavelengths for a given initial condition and pulse characteristic. We can ask if the different intensity distributions operate simultaneously enlarging the laser bandwidth or if each transverse mode competes with the other during the pulse and the

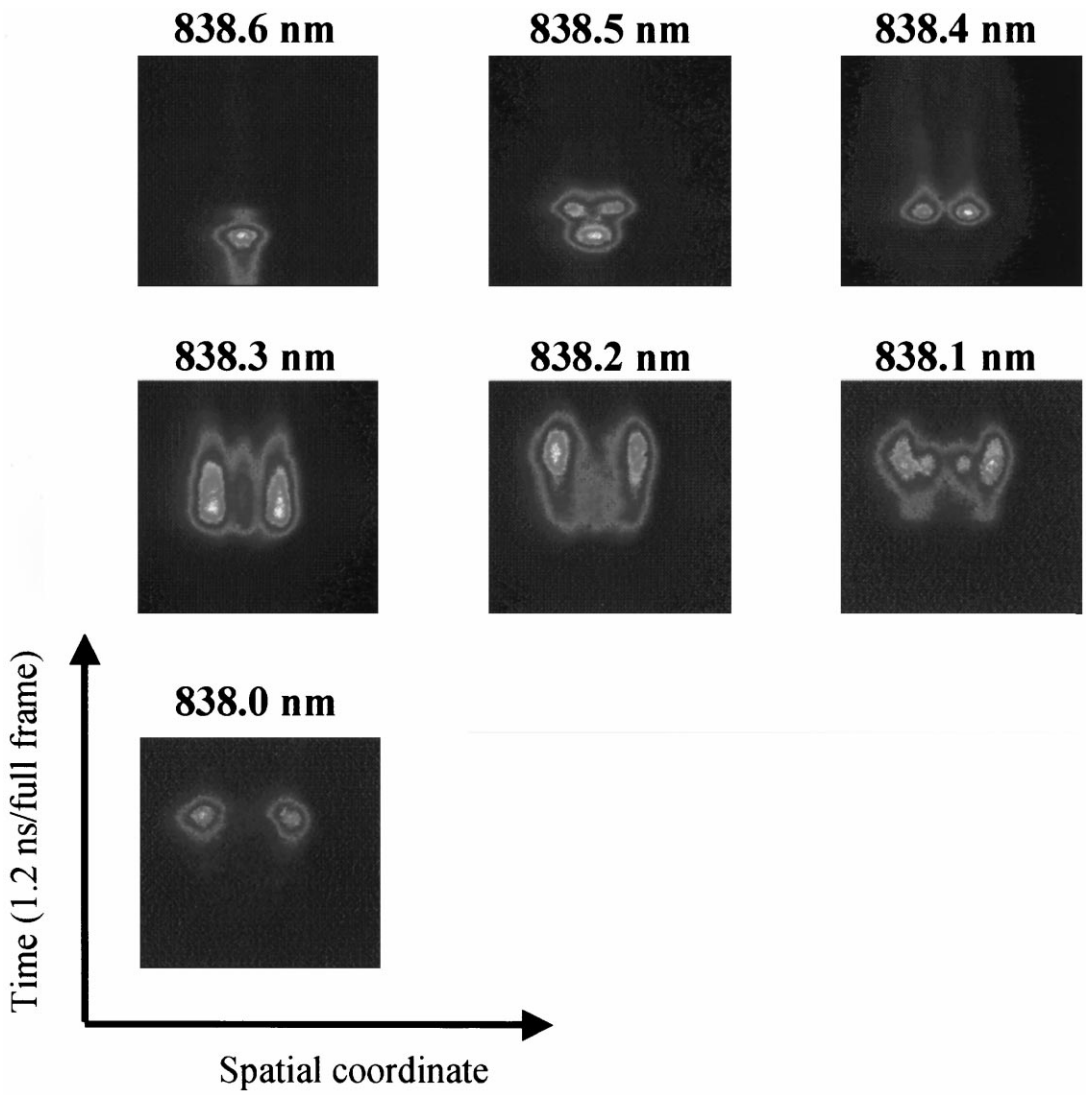

Fig. 4. Time-resolved horizontal cross-sections of the laser beam at different wavelengths. The VCSEL active region is 22 μm in diameter, it is DC biased at $1.03 \times I_{th}$ and it is excited by a pulse of 600 ps width and $6 \times I_{th}$ amplitude. The time span is 1.235 ns. The intensity is represented on a grey scale. The maximum level is different for each picture in order to enhance the contrast. Black corresponds to zero intensity level (background), while white corresponds to the following intensity levels (arbitrary units): 150 for 838.6 nm, 500 for 838.5 nm, 2500 for 838.4 nm, 1000 for 838.3 nm, 1000 for 838.2 nm, 1000 for 838.1 nm, 200 for 838 nm.

laser operates at a single wavelength at each time. Unfortunately it was technically impossible for us to detect simultaneously a two-dimensional intensity distribution and the time-resolved intensity at each local position. However, we were able to perform an unidimensional measurement. We resolved both wavelength and intensity as a function of time at each point of the unidimensional section.

To obtain the data shown in Fig. 3, the laser was initially biased below threshold and radiation emission was observed as the excitation pulse was applied. The streak camera was triggered by the excitation pulse and the detection system allowed to measure the intensity as a function of time at each preselected frequency, as explained above.

We immediately notice from Fig. 3 that lower-order modes appear first. However, they disappear relatively fast as the peak current increases, leading to the appearance of higher-order modes. At this stage there is a dominant

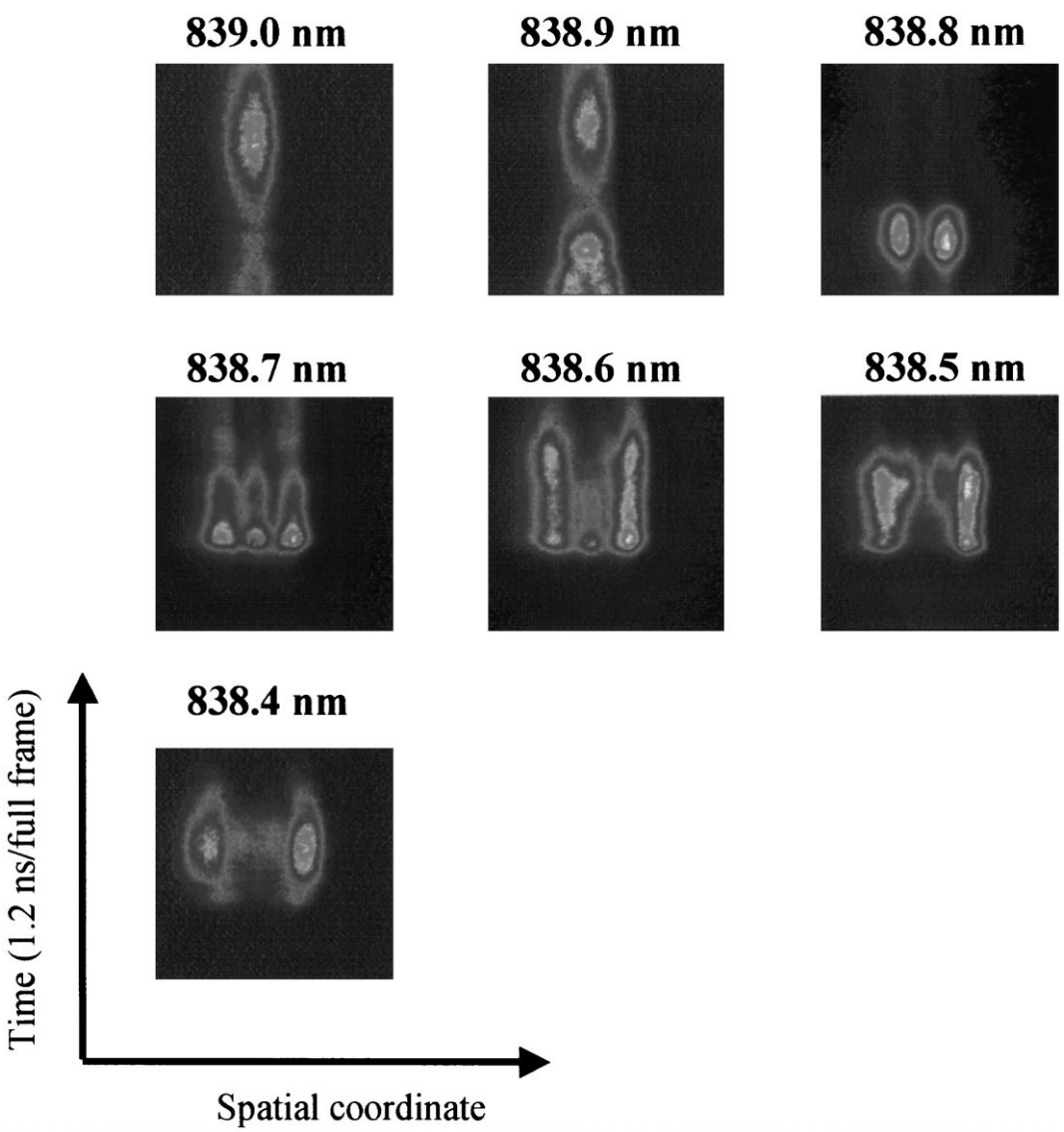

Fig. 5. Time-resolved horizontal cross-sections of the laser beam at different wavelengths. The VCSEL active region is 22 μm in diameter, it is DC biased at $1.7 \times I_{th}$ and excited by a pulse of 600 ps width and $6 \times I_{th}$ amplitude. The time span is 1.235 ns. The intensity is represented on a grey scale. The maximum level is different for each picture in order to enhance the contrast. Black corresponds to zero intensity level (background), while white corresponds to the following intensity levels (arbitrary units): 500 for 839.0 nm, 1500 for 838.9 nm, 3000 for 838.8 nm, 2000 for 838.7 nm, 700 for 838.6 nm, 200 for 838.5 nm, 125 for 838.4 nm.

spatial structure persisting over the whole duration of the pulse. Other intensity distributions coexist with it, but they usually compete and they reach their maximum intensity at different times progressing from high to low wavelengths. Thus this chirping is produced by the time-dependent excitation. After the excitation pulse ends, the laser switches off directly from higher-order modes, suggesting a bistable behavior between different spatial structures close to threshold. This phenomena could be associated with the dynamical sweep of the pump parameter [18,19] rather than a true bistability. These results are in agreement with Refs. [11,12] where bistable behavior was also observed between the TEM_{00} and TEM_{01} modes for switch-on of a VCSEL. Fig. 3 shows a strong competition among different patterns in general giving rise to a relatively large emission bandwidth but mainly centered, after a fast transient, at a constant frequency.

We also notice that the wavelength at which each transverse mode switches off at the end of excitation pulse is red shifted by 0.1 nm from the wavelength at which it switches on during the excitation pulse. This chirp of each mode can be easily understood considering the change of the index of refraction due to the variation of carrier density [20,21].

Similar measurements were also performed for a bias current above laser threshold. In this situation we distinguish two cases: the laser operating in a single TEM_{00} mode or in two modes (TEM_{00} and TEM_{01}) simultaneously prior to the excitation pulse. In the first case (Fig. 4) we observe an increase of the TEM_{00} intensity and a blue shifting of its wavelength during the first phase of the excitation pulse. Immediately after, higher-order modes appear with a consequently shift in wavelength towards the blue side of the spectrum. The time span of our measurements is 1235 ps, and the width of the excitation pulse was 600 ps. So it is evident from the records shown in Fig. 4 that, after the pulse, there is an interval where the VCSEL does not emit anymore at any wavelength. Thus, VCSEL does not recover, at the pulse end, its initial state, or the non-lasing state coexists with the single TEM_{00} mode. We then set the laser such that it operated with two modes at two different wavelengths prior to the pulse (Fig. 5). During the first part of the excitation pulse we notice that there is a fast sweep towards shorter wavelengths of the low-order modes, until they disappear. A higher-order mode dominates during the excitation pulse but it coexists with other modes always on the blue side of the spectrum. However, the time evolution of each wavelength seems to indicate that the system still does not relax to its initial state even if the excitation pulse is shorter than the recording time; this result may be interpreted in terms of spatial hole burning [22].

Further experimental tests should be done in the future to study the interplay betweeen the transverse effects and the polarization of the electromagnetic field. It is interesting from the scientific point of view to explain the frequency shifting towards the blue side of the spectrum. It could be understood as a simple generation of complex patterns involving the participation of high-order modes which lie always on one side of the fundamental one. However, the fact that the initial state is not recovered after the pulse ends leaves a question open on this subject. Comparative measurements with cw multitransverse mode lasers may clarify this issue of pattern formation and the dynamical evolution of operating frequencies as control parameter are changed.

Acknowledgements

MG and JRT acknowledge contract CI 1∗CT93-0331 of the EEC. MG acknowledges the EU, TMR Program. The authors of the Colorado State University acknowledge the support of the NSF Optoelectronic Computing System Center. CSM also acknowldeges the support of the National Science Foundation Career Award, ECS 95-02888. We thank J.L.A. Chilla for precious help and O.F. Buccafusca for helpful discussions.

References

[1] See, e.g., Special Issue on Transverse Effects in Optical Systems, N.B. Abraham, W. Firth (Eds.), J. Opt. Soc. Am. B, June 1990.
[2] J.R. Tredicce, E. Quel, C. Green, A. Ghazzawi, L.M. Narducci, M. Pernigo, L.A. Lugiato, Phys. Rev. Lett. 62 (1989) 1274.
[3] C. Green, G.B. Mindlin, E.J. D'Angelo, H. Solari, J.R. Tredicce, Phys. Rev. Lett. 65 (1990) 3124.
[4] P. Coullet, L. Gil, F. Rocca, Optics Comm. 73 (1989) 403.
[5] F.T. Arecchi, G. Giacomelli, P. Ramazza, S. Residori, Phys. Rev. Lett. 67 (1991) 3749.
[6] G. Huyet, C. Martinoni, J.R. Tredicce, S. Rica, Phys. Rev. Lett. 75 (1995) 4027.
[7] G. Huyet, J.R. Tredicce, Physica D 96 (1996) 209.
[8] C.J. Chang-Hasnain, M. Orenstein, A. Von Lehmen, L.T. Florez, J.P. Harbison, N.G. Stoffel, Appl. Phys. Lett. 57 (1990) 218.
[9] K. Tai, Y. Lai, K.F. Huang, T.C. Huang, T.D. Lee, C.C. Wu, Appl. Phys. Lett. 63 (1993) 2624.
[10] H. Li, T.L. Lucas, J.G. McInerney, R.A. Morgan, Chaos, Solitons Fractals 4 (1994) 1619.
[11] O. Buccafusca, J.L.A. Chilla, J.J. Rocca, S. Feld, C. Wilmsen, V. Morozov, R. Leibenguth, Appl. Phys. Lett. 68 (1996) 590.
[12] O. Buccafusca, J.L.A. Chilla, J.J. Rocca, C. Wilmsen, S. Feld, R. Leibenguth, Appl. Phys. Lett. 67 (1995) 590.
[13] J. Martin-Regalado, S. Balle, M. San Miguel, Optics Lett. 22 (1997) 460.
[14] E.J. D'Angelo, E. Izaquirre, G.B. Mindlin, G. Huyet, L. Gil, J.R. Tredicce, Phys. Rev. Lett. 68 (1992) 3702.
[15] G. Huyet, C. Mathis, H. Grassi, J.R. Tredicce, N.B. Abraham, Optics Comm. 111 (1994) 488.

[16] J. Martin-Regalado, M. San Miguel, N.B. Abraham, F. Prati, Optics Lett. 21 (1996) 351.
[17] G. Dangelmayr, E. Knobloch, Non Linearity 4 (1991) 399; the same equation applied to lasers has been used in Ref. [14].
[18] P. Mandel, E. Erneux, Phys. Rev. Lett. 53 (1984) 1818.
[19] P. Mandel, in: R. Pike, S. Sarkar (Eds.), Frontiers of Quantum Optics, Adam Hilger, Bristol, 1986, 450 pp.
[20] B.R. Bennet, R.A. Soref, J.A. DelAlama, IEEE J. Quantum Electron. QE-26 (1990) 113.
[21] A. Olsson, C.L. Tang, Appl. Phys. Lett. 39 (1981) 24.
[22] J.Y. Law, G.P. Agrawal, Optics Comm. 138 (1997) 95.